Processing and Application of Ceramics 12 [2] (2018) 143–152
https://doi.org/10.2298/PAC1802143K

Impact of B_2O_3 and La_2O_3 addition on structural, mechanical and biological properties of hydroxyapatite

Sina Khoshsima[1], Ammar Z. Alshemary[2], Aysen Tezcaner[1,3], Sedat Surdem[4], Zafer Evis[1,3,*]

[1]*Biomedical Engineering, Middle East Technical University, Ankara 06800, Turkey*
[2]*Biomedical Engineering, Karabuk University, Karabuk 78050, Turkey*
[3]*Engineering Sciences, Middle East Technical University, Ankara 06800, Turkey*
[4]*National Boron Research Institute, Ankara, 06520, Turkey*

Received 22 November 2017; Received in revised form 24 March 2018; Accepted 27 May 2018

Abstract

In this study, hydroxyapatite-B_2O_3-La_2O_3 composites (with ≤ 20 wt.% B_2O_3 and ≤ 2 wt.% La_2O_3) were synthesized via wet precipitation method and calcined at 1100 °C for 1 h. X-ray diffraction (XRD) analysis revealed the existence of the pure hydroxyapatite (HA) phase with high crystallinity. Characteristic absorption bands of HA were also observed in Fourier transform infrared spectra. Furthermore, scanning electron microscopy images demonstrated that the addition of B_2O_3 and La_2O_3 into HA enhanced the particle growth. Mechanical properties of the composites were studied by diametral tensile test and the results showed that incorporation of 10 wt.% B_2O_3 and 2 wt.% La_2O_3 led to a 39% increase in tensile strength (compared to the pure HA). In vitro cytocompatibility of HA-B_2O_3-La_2O_3 composites was investigated using Osteosarcoma Cell Lines (Saos-2). Incorporation of B_2O_3 and La_2O_3 into HA had no toxic effect towards the cells. Based on its tensile strength properties and biological response, composite of 88 wt.% HA, 10 wt.% B_2O_3 and 2 wt.% La_2O_3 was suggested as a promising composite for bone tissue engineering applications.

Keywords: *biocomposites, hydroxyapatite, B_2O_3, La_2O_3, microstructure, tensile strength, Saos-2 cells*

I. Introduction

Hydroxyapatite (HA, $Ca_{10}(PO_4)_6(OH)_2$) is a biocompatible and bioactive material that is used in different biomedical applications because of its structural similarity to bone mineral. HA has been found to have limited orthopaedics applications due to its brittle nature and low tensile strength. Thus, HA-based composites need an improvement in strength and toughness to be used as implant materials. The addition of metal oxides into HA, such as MgO [1], Al_2O_3 [2], ZrO_2 [3], Nb_2O_5 [4], ZnO [5], Bi_2O_3 [6] and many others, have been done to improve its mechanical or structural characteristics [7]. There are a few studies [8–11] which already revealed that the inclusion of a metal oxide might act as reinforcing agent, but at the same time, it may decompose HA into tricalcium phosphate (TCP). This decomposition has negative influences on densification and mechanical properties of HA [8,9,11].

*Corresponding author: tel: +90 312-210 4450,
fax: +90 312-210 4462, e-mail: *evis@metu.edu.tr*

It has been reported that boron oxide (B_2O_3) augments the wound healing process [12] and has pivotal roles and functions in bone physiology [13]. However, doping of HA with B_2O_3 is scarcely recognised in such reports. Mixing of about 5% B_2O_3 into HA might increase the flexural strength up to 58 MPa as well as the Vickers micro-hardness which can be around 2.1 GPa [11]. In another study, Lee *et al.* [14] reported that the addition of B_2O_3 into bioglass structure increased the osteointegration with no sign of toxicity. Yang *et al.* [15] showed that the addition of B_2O_3 to SiO_2-CaO-P_2O_5 increased its degradation rate and bioactivity.

In addition, lanthanum oxide (La_2O_3) is another vital oxide that can be used for improving properties of HA. It was reported [16] that HA-2.5 La_2O_3 composite had higher hardness value than the pure HA which was attributed to the low porosity, high grain size and a low glassy phase in the composite. Henceforth, La_2O_3 was substituted at a low amount and no suppression of bioactivity was observed for this doping [17]. Aside, La_2O_3 added into the silicates resulted in higher elastic modu-

lus and hardness [17]. Additionally, it improved tensile and bending strengths of HA [18]. Indeed, an infiltration of a fibrous tissue with no noteworthy sign of inflammation was observed for La-containing HA discs after implantation into the bones of a rat [18,19]. Fernandez *et al.* reported [18,20] that incorporation of 140-lanthanum into the apatite structure played a vital role in increased resistance of the hard tissues to acid dissolution.

In this study, microstructural and mechanical characteristics of HA-B_2O_3-La_2O_3 synthesized by co-precipitation method were evaluated. To the best of our knowledge, no study yet had been reported for the co-substitution of B_2O_3 and La_2O_3 into HA structure. Moreover, *in vitro* cytocompatibility of doped HA using Saos-2 cell line was also investigated.

II. Materials and methods

2.1. Preparation of HA and HA-B_2O_3-La_2O_3

Calcium nitrate tetrahydrate ($Ca(NO_3)_2 \cdot 4\,H_2O$) (Merck, Germany) and di-ammonium hydrogen phosphate ($(NH_4)_2HPO_4$, Merck, Germany) were used as Ca^{2+} and PO_4^{3-} sources, respectively. Ammonia solution (NH_4OH, Merck, Germany) was used to adjust the pH and B_2O_3 (Sigma-Aldrich, Germany) and La_2O_3 (Aldrich, Germany) were used to prepare HA-B_2O_3-La_2O_3 composites.

HA was synthesized by the co-precipitation method using 0.5 M calcium nitrate and 0.3 M di-ammonium hydrogen phosphate which were previously dissolved in distilled water separately and then their pH was adjusted above 10 with NH_4OH. The Ca/P ratio was kept at 1.67 to produce stoichiometric HA. Di-ammonium hydrogen phosphate solution was added dropwise into continuously stirred calcium nitrate solution. After stirring the HA solution for 2–3 h, it was heated at 90 °C for 1 h, then stirred for 1 day more at room temperature. The solution was filtered through a fine filter paper and washed several times to remove the remaining ammonia. The filtered wet cake was dried at 200 °C in an oven overnight to remove the excess water. Finally, the dried HA particles were ground to fine powder and calcined at 1100 °C for 1 h.

In order to synthesize HA-B_2O_3-La_2O_3 composites, the precursor powders were weighed according to the defined ratio (Table 1), mixed in pure ethanol and left for stirring for 3–5 h to obtain the best composite structure. The obtained mixture was then dried overnight to remove the excess alcohol and milled/mixed in a mortar and pestle to achieve the perfect distribution. After that, the composite powders were pressed and sintered at 1100 °C for 1 h. The prepared composites were denoted as *x*HA*y*B*z*La, where *x*, *y* and *z* are portions of HA, B_2O_3 and La_2O_3 in composites, respectively.

Table 1. Nominal composition of pure HA and HA-B_2O_3-La_2O_3 composites

Sample ID	HA [wt.%]	B_2O_3 [wt.%]	La_2O_3 [wt.%]
HA	100	0	0
90HA10B	90	10	0
88HA10B2La	88	10	2
80HA20B	80	20	0
78HA20B2La	78	20	2

2.2. Characterization

The phase purity of HA-B_2O_3-La_2O_3 composites was determined by using X-ray diffraction technique (XRD, Bruker D8) operated at 40 kV and 40 mA utilizing Cu Kα radiation between 2θ angles from 20° to 70° with 2.0°/min resolution. The degree of crystallinity was calculated according to the fraction of crystalline phase from X-ray diffraction data by using following equation [21]:

$$X_C = 1 - \frac{V_{112/300}}{I_{300}} \cdot 100 \tag{1}$$

where X_C is the degree of crystallinity, I_{300} is the intensity of 300 reflection and $V_{112/300}$ is the intensity of the hollow between 112 and 300 reflection. Lattice parameters were calculated using an UnitCell software [22,23].

Fourier transform infrared spectroscopy (FTIR) analysis was conducted to study the functional groups with the infrared spectra measurements in the range of 4000–400 cm^{-1} (Bruker IFS66/S). Morphology and surface microstructure of HA-B_2O_3-La_2O_3 composites were investigated using scanning electron microscopy (SEM, LEO 1430VP). The average grain size of the sintered samples was determined from the SEM images. Intercept method was used to determine the grain size of the sintered samples [24,25].

2.3. Disc shaping and sterilization

Initially, HA-B_2O_3-La_2O_3 powders (670 mg) were uniaxially pressed into discs (14 mm × 2 mm) using automatic hydraulic machine (Carver, Inc.) at 10 kN load for 1 minute, then sintered at 1100 °C for 1 h prior to their use for mechanical analysis. Discs were sterilized at 200 °C for 2 h before performing *in vitro* cytotoxicity test.

2.4. Mechanical analysis

Density (ρ_a) of the sintered composites was determined by measuring their dry weight (m) and calculating the volume (V) obtained from the pellet dimensions using the following formula:

$$\rho_a = \frac{m}{V} \tag{2}$$

Theoretical density of the composites (components *a* (HA), *b* (B_2O_3) and *c* (La_2O_3)) was calculated using the densities (ρ), and known weights (W) via the following formula:

$$\rho_{com} = \frac{W_a + W_b + W_c}{\frac{W_a}{\rho_a} + \frac{W_b}{\rho_b} + \frac{W_c}{\rho_c}} \tag{3}$$

The relative density of the composites was calculated by dividing the measured density with a theoretical density

of each composite. Theoretical density of the pure HA is 3.156 g/cm^3.

The porosity of HA-B_2O_3-La_2O_3 discs was determined by mercury intrusion porosimetry (MIP, AutoPore IV 9520, Micyromeritics Instrument). The samples were subjected to a pressure range of 50–60000 psi which can give measurements for pores of radii from 3 nm to 360 μm.

The Vickers micro-hardness (HV) measurements were determined using a Vickers micro-hardness tester (HMV-2, Shimadzu, Japan). Approximately 20 measurements were performed on each sample with a diamond indenter at 1.968 N load for 20 seconds. The average micro-hardness was calculated by the following formula:

$$HV = 0.001854 \cdot \frac{P}{d^2} \quad (4)$$

where HV is the value of micro-hardness, P stands for the amount of load applied to the sample and d is the length of indent diagonal.

The diametral tensile tests of the sintered discs were performed by a universal testing machine (LS 500, Llyod Instruments, UK). The disc was compressed diametrically between two parallel plates. During the compression, a maximum tensile strength was generated across the flat surface keeping diameters of the discs normal to the loading direction. The tensile strength of the samples was calculated with the following formula [24,26]:

$$S = \frac{2F}{\pi \cdot D \cdot t} \quad (5)$$

where F is failure force, D is sample diameter and t is the sample thickness. The diametral tensile test was conducted in triplicates for each experimental group ($n = 3$). In order to evaluate the machinability of the specimens, drilling test was performed on the pellets. The machining device was a 3-axis system with a spindle speed of 600 rpm. A 0.05-inch twist drill bit was used to test the samples. Machinability test of the discs was performed in duplicates for each group.

2.5. In vitro cytotoxicity evaluation

In vitro cytotoxicity studies were conducted using Saos-2 cells (human osteosarcoma cell line). In this work, the Saos-2 cells were grown in high glucose Dulbecco's modified Eagle medium (DMEM), further supplemented with 10% fetal bovine serum (FBS) and 0.3% Penicillin-Streptomycin. The initial cell seeding density was 5×10^4 cells/disc. The cells were incubated on composite discs in a carbon dioxide incubator (5215, Shell Lab, USA) at 37 °C under 5% CO_2 humidified environment. The medium was refreshed every 2 days. The proliferation of the cells on the discs was analysed by PrestoBlue™ viability assay at different incubation periods (1, 3 and 7 days). At each time point, PrestoBlue™ viability reagent was added to wells containing cell seeded discs and then the well plates were incubated at 37 °C under 5% CO_2 environment for 20 h. During incubation PrestoBlue™ reagent was reduced into intensely coloured formazan, as a result of enzymatic activity of the viable cells. After 20 h of incubation, the medium in each well was collected and their absorbance was read by μQuant™ spectrophotometer (Biotek Instruments Inc., USA) with an excitation wavelength of 570 nm and an emission wavelength of 600 nm. The amount of metabolic reduction caused by cells was then calculated. After collection of the medium, cells were washed with PBS once more and growth medium was added for further culturing of cells. The viability of cells seeded on tissue culture plate was used as positive control. All experiments were performed in quadruplicate. The measured data were expressed as a mean value with corresponding standard deviation. One-way analysis of variance (ANOVA) was carried out with Tukey's Multiple Comparison Test for the *post hoc* pairwise comparisons using SPSS-15.0 Software (SPSS Inc., USA). Differences were considered as significant for $p \leq 0.05$.

Morphology of Saos-2 cells on composite discs was investigated using SEM analysis. Two samples for each composition were seeded with cells at an initial seeding density of 5×10^4 cells/disc. After 1 and 7 days of incubation, the medium was removed, and the cells were washed with phosphate buffered saline (PBS) and then fixed with 3% glutaraldehyde in PBS for 15 minutes. After fixation, the cells were washed with PBS and dehydrated with graded ethanol-water solution series (30, 50, 70, 80, 90 and 100%) and hexamethyldisilazane (HMDS). The experiments were achieved in duplicates for each group. Prior to SEM analysis, discs were coated with gold-palladium via precision etching coating system (PECS, Gatan 682, USA) to a thickness of 5 nm.

III. Results and discussion

3.1. Structural analysis

XRD patterns of the HA-B_2O_3-La_2O_3 composites sintered at 1100 °C are given in Fig. 1. All the patterns showed the characteristic peaks of HA and they were in good agreement with stoichiometric HA (JCDPS No: 09-432). No β-TCP peaks around 31.03° were observed, which confirmed the phase purity of HA. XRD pattern showed the incorporation of B_2O_3 and La_2O_3 in the HA structure (90HA10B and 88HA10B2La) and there was no decomposition of HA into biphasic or triphasic calcium phosphate. Peaks located at 27.67° and 29.98° belong to (310) and (222) diffraction planes and they are in good agreement with B_2O_3 structure (JCPDS No: 06-0297). The intensity of XRD peaks indicated an increase in the crystallinity of composites which could be ascribed to the incorporation of La_2O_3 in HA [27]. Similarly, a small peak appearing around 29.91° for 88HA10B2La composite is attributed to the (101) diffraction plane and assigned to the incorporation of La_2O_3 in the HA sample. This result corresponds to standard La_2O_3 (JCPDS No: 05-0602). In the XRD pat-

tern of 80HA20B composite a small peak observed at 30.57° might belong to the diffraction plane (113) and according to standard (JCDPS No: 26-0347) it refers to calcium borate ($Ca_3B_2O_6$). Calcium borate formation can be explained according to the following reactions (Eq. 6a-c) [28–31]:

$$Ca^{2+} + 2\,OH^- \xrightarrow{50-100\,^\circ C} Ca(OH)_2 \quad (6a)$$

$$Ca(OH)_2 \xrightarrow{>350\,^\circ C} CaO + H_2O \quad (6b)$$

$$3\,CaO + B_2O_3 \longrightarrow Ca_3B_2O_6(s) \quad (6c)$$

Calcium borate is identified as a potential anti-inflammatory agent, therefore, it can be considered as a beneficial additive in the samples [32]. Noticeable decrease in intensity of the peaks was observed and this decrease could be interpreted as the lower crystallinity of 78HA20B2La sample compared to other composites (Table 2). The amount of B_2O_3 and La_2O_3 incorporated together may be one of the reasons for the decomposition of HA structure into β-TCP and CaO (Eq. 7) [33]:

$$Ca_{10}(PO_4)_6(OH)_2 \longrightarrow 3\,\beta\text{-}Ca_3(PO_4)_2 + CaO + H_2O \quad (7)$$

However, amount of β-TCP formed was still lower compared to other previous studies conducted on ZrO_2 and Al_2O_3-HA composites [8,9].

Lattice parameters of the pure HA and HA-B_2O_3-La_2O_3 composites are summarized in Table 2 and the lattice values were in good agreement with dimensions of hexagonal structure of HA. Few variations in a and c axis of HA-B_2O_3-La_2O_3 composites could be attributed to the dehydroxylation of the hydroxyl group which is very common for the samples calcined at high temperatures [34] or due to the partial substitution of a smaller radius Ca^{2+} (0.99 Å) with a larger radius La^{3+} ion (1.17Å) [18]. However, the addition of both B_2O_3 and La_2O_3 into HA did not result in significant changes in XRD patterns of the HA as they were still matched with the standard JCPDS file for HA.

FTIR spectra of the pure HA and HA-B_2O_3-La_2O_3 composites are illustrated in Fig. 2. The pure HA spectrum showed an absorption peak at the position of 474 cm^{-1} which was attributed to $\nu_2(PO_4^{3-})$ group. Another two absorption peaks located at 1056 and 1096 cm^{-1} were attributed to $\nu_3(PO_4^{3-})$ group, the peak positioned at 962 cm^{-1} was allocated to $\nu_1(PO_4^{3-})$ group. Besides these peaks, two absorption peaks located at 571 and 601 cm^{-1} were assigned to $\nu_4(PO_4^{3-})$ group. OH^- groups were detected in HA structure in two sites (630 and 3572 cm^{-1}) corresponding to bending and stretching modes of OH^- group, respectively. In addition to the stretching and deformation vibrational modes of PO_4^{3-} groups, a tiny peak with low intensity was observed at 1460 cm^{-1} which is related to the CO_3^{2-} group. This result may be affected by contaminants during the synthesis process. A gradual decrease in the intensity of the OH^- band was observed indicating the partial dehydration of HA as a result of sintering at 1100 °C.

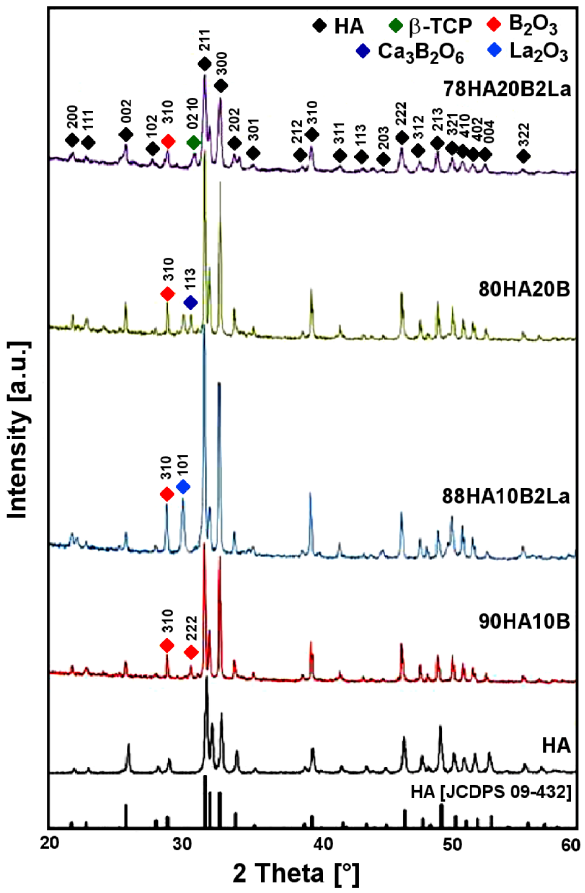

Figure 1. XRD patterns of pure HA and HA-B_2O_3-La_2O_3 composites sintered at 1100 °C

Table 2. Lattice parameters and degree of crystallinity of pure HA and HA-B_2O_3-La_2O_3 composites

Sample ID	Lattice Parameters			X_C [%]
	a-axis [Å]	c-axis [Å]	Cell volume [Å^3]	
Standard HA	9.418	6.884	528.8	-
HA	9.407	6.882	527.4	90
90HA10B	9.405	6.880	527.0	93
88HA10B2La	9.399	6.879	526.3	96
80HA20B	9.389	6.894	526.3	94
78HA20B2La	9.389	6.879	525.2	83

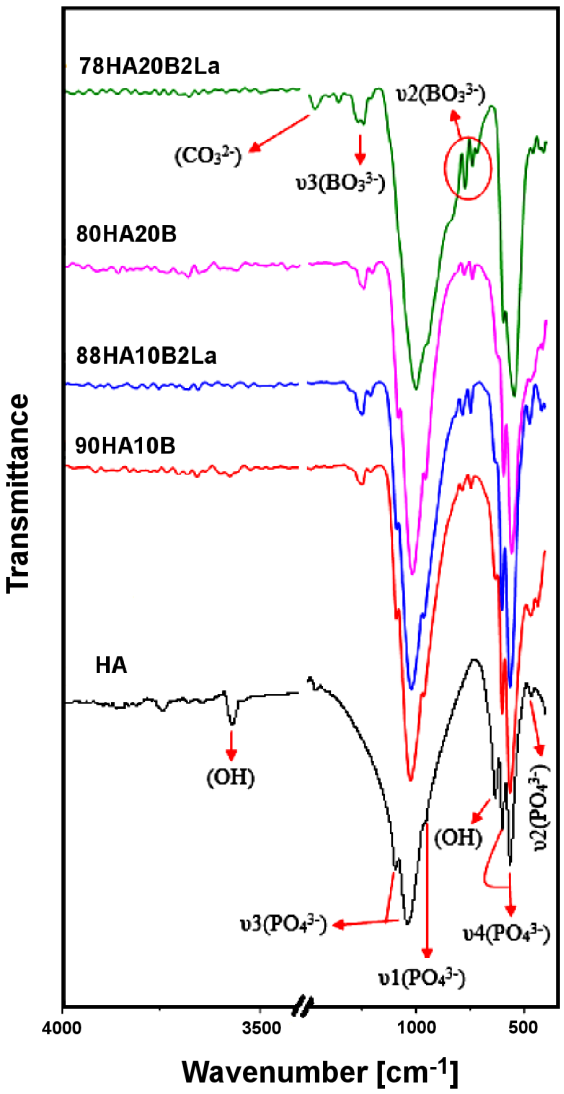

Figure 2. FTIR spectra of pure HA and HA-B_2O_3-La_2O_3 composites sintered at 1100 °C

The increased sharpness of PO_4^{3-} peaks due to the doping of B_2O_3 and La_2O_3 could be associated with the highly crystalline structure as confirmed by the XRD results (Fig. 1). Along with absorption peaks of the pure HA, other peaks were detected at 742 and 780 cm^{-1}, which could be assigned to the $\nu_2(BO_3^{3-})$ symmetric bending. Similarly, absorption band in the range of 1205–1245 cm^{-1} was attributed to the asymmetric stretching ν_3 mode of BO_3^{3-} group [35].

Surface morphologies of the pure HA and HA-B_2O_3-La_2O_3 composites were examined by SEM (Fig. 3). SEM images showed that particles of the pure HA were densely packed and the grain size was 192 nm, as illustrated in our previous study [36]. Micrograph images confirmed that incorporation of B_2O_3 resulted in an increase in the porosity as well as in the grain size (342 nm and 364 nm for the 90HA10B and 80HA20B samples, respectively). The results are in good agreement with the previous studies [37,38]. Likewise, the introduction of La_2O_3 into the HA resulted in no big difference in the morphology, however, a larger grain size (615 nm) was observed. Our results are in good agreement with the previous studies [39,40]. The crystallinity of the 78HA20B2La composite showed less improvement compared to other groups, furthermore, it showed highly porous structure (Table 3). However, as reported by previous studies, an interconnected porous structure is extremely important for hard tissue applications [41].

3.2. Mechanical analysis

Density and relative density of the materials are summarized in Table 3. Relative density of the pure HA was decreased by addition of B_2O_3 and La_2O_3. The presence of weak interphases of B_2O_3 and La_2O_3 particles in between HA particles prevented HA particles to sinter. Moreover, this hindered sintering upon increasing amount of dopant led to the reduced relative density [42]. Furthermore, the relative density is considered as a vital biomaterial parameter owing to its significant effect on potential for steric hindrances to cell motility [43]. It is reported that the material with lower relative density enhanced NR6 fibroblasts cell migration within the scaffold variants [44].

Vickers micro-hardnesses of the pure HA and HA-B_2O_3-La_2O_3 composites are given Fig. 4a. The pure HA exhibited the highest hardness of 5.13 GPa. However, the hardness of the pure HA sharply decreased with an addition of B_2O_3 and La_2O_3. These decreases in micro-hardness value were presumably due to the highly porous nature (Table 3) [45] and increase in the grain size of the HA-B_2O_3-La_2O_3 composites (Fig. 3) [46].

Diametral tensile strength results are illustrated in Fig. 4b. It was observed that the 88HA10B2La and 80HA20B composites exhibited the highest tensile strength in comparison to other compositions which could be due to a high degree of crystallinity. Tensile strength increases with increasing degree of crystallinity [47,48]. Similarly, the 78HA20B2La sample showed the lowest tensile strength value which could be due to the

Table 3. Relative density and porosity values of the materials sintered at 1100 °C for 1 h

Sample ID	Sintered density [g/cm^3]	Relative density [%TD]	Porosity [v/v%]
HA	2.91	92	8
90HA10B	2.82	89	11
88HA10B2La	2.75	87	13
80HA20B	2.33	74	26
78HA20B2La	2.41	76	24

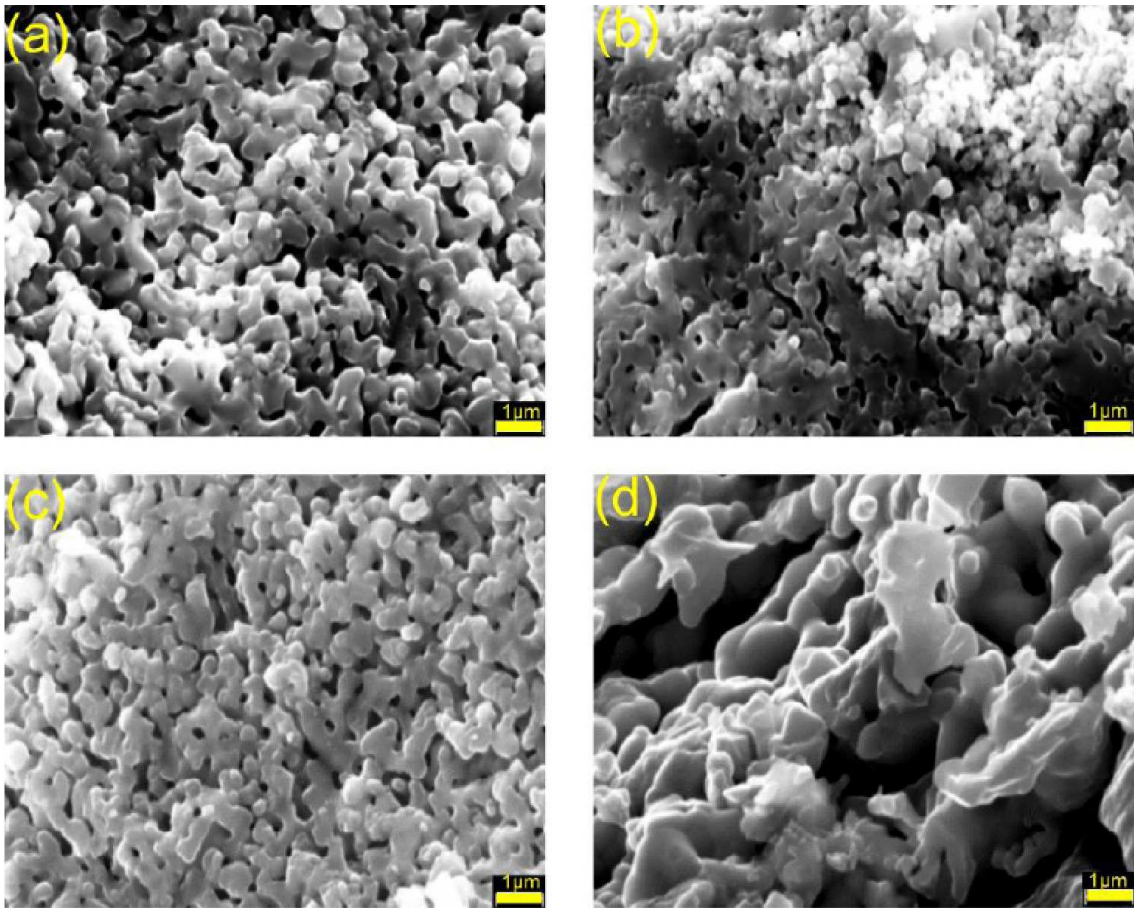

Figure 3. SEM images of: a) 90HA10B, b) 88HA10B2La, c) 80HA20B and d) 78HA20B2La composites

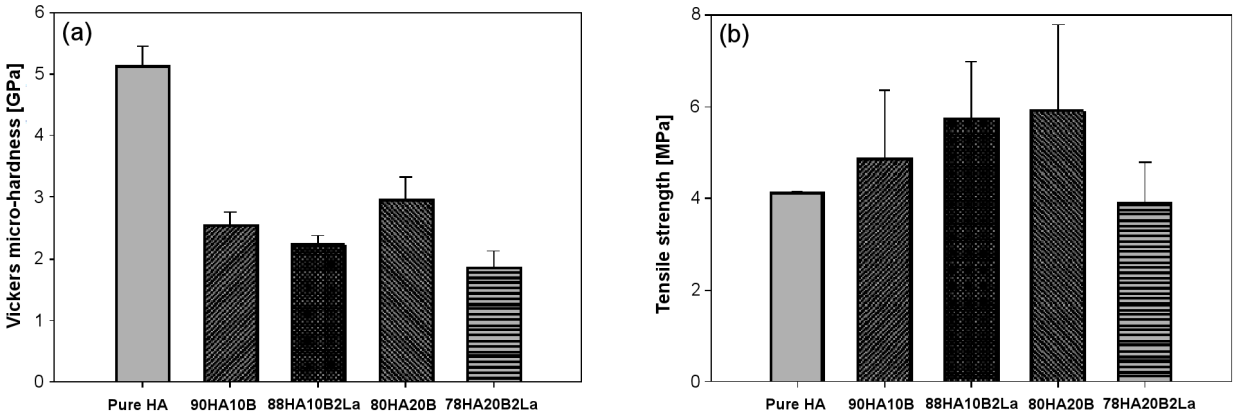

Figure 4. Vickers micro-hardness (a) and diametral tensile strength (b) of pure HA and HA-B_2O_3-La_2O_3 composites

reduction in the degree of crystallinity (Table 2). In addition, it was reported that the presence of a second phase had a considerable effect on the tensile strength that might decrease the mechanical properties of ceramics [24]. Moreover, our result was far away from dense HA [49] which could be due to the porous nature of HA-B_2O_3-La_2O_3 composites as observed in SEM images (Fig. 3) [26].

The bioceramics used in hard tissue engineering should possess good machining capacity, as they should be frequently subjected to redesign during orthopaedic surgery. Figure 5 presents the samples after drilling test. None of the composite discs break during the process while HA one broke, as illustrated in our previous study [36]. This behaviour could be attributed to the brittle nature of HA, and similar observations were reported in literature [42]. Thus, the composites are machinable with no evidence of large-scale cracking or chipping. The key reason for the enhanced machinability of ceramic composites could be due to many issues such as: i) the uniform distribution of lanthanum [50], ii) the creation of weak interphases of B_2O_3 and La_2O_3 particles in between the HA particles [42] (tthese interphases of B_2O_3 and La_2O_3 particles induce interfacial de-bonding

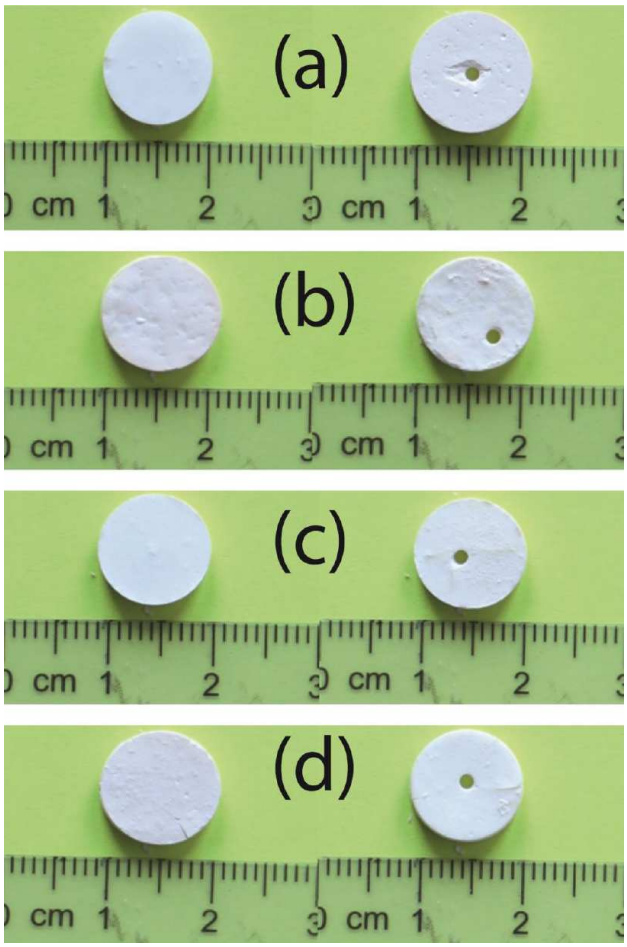

Figure 5. Images of discs before (left) and after (right) the drilling test: a) 90HA10B, b) 88HA10B2La, c) 80HA20B and d) 78HA20B2La

and crack deflection during drilling, thus led to the inhibition the crack growth [42]), iii) the porous nature of HA-B_2O_3-La_2O_3 composites (it is known that the porosity plays a vital role in the optimal machinability during which pores could have prevented the catastrophic destruction of materials during drilling through crack defection [51]) and iv) the presence of secondary phases.

3.3. In vitro cytotoxicity evaluation

HA is well known as a biocompatible material and has no toxic influence on osteosarcoma cells (Saos-2) [52]. However, our main interest was to evaluate the impact of B_2O_3 and La_2O_3 addition on biological properties of HA. Thus, Saos-2 cell proliferation was evaluated using PrestoBlue™ viability assay (Fig. 6). The results showed that the cell viability on HA discs after one day was statistically higher than all samples except the composite 88HA10B2La. On days 3 and 7 cell viability on all composite discs was statistically lower than the one observed on HA discs.

After one day the highest cell viability was observed on the HA and 88HA10B2La [53]. There was no statistical difference between the HA and 88HA10B2La in terms of cell viability at day 1 which could be due to highly crystalline structure of the composite 88HA10B2La in comparison with other samples and it was assigned to the enhanced crystallinity of the sample (Table 2). Increased crystallinity might have inhibited the degradation rate of HA-B_2O_3 structure as a result of low ionic exchange with the environment [54]. Cells viability observed in other composite groups was statistically lower than observed on HA discs. Incorporation of 10 wt.% and 20 wt.% of B_2O_3 in HA showed slightly toxic effect. It was reported that incorporation of La^{3+} increased the proliferation rate of MC3T3-E1 cells [18,55]. For all composites, a time-dependent decrease in the cell viability was observed. This could be due to the initial confluences reached at some areas on discs after cell seeding. However, only on boron doped discs, cell viability significantly decreased with time and cell viability decreased to a level of 20% which indicates that boron ion dissolution caused a toxic effect in cells. Among the composites, cell viability on the 88HA10B2La decreased only 20% after 7 days and is comparable with the TCP sample. Therefore, this group can be considered as cytocompatible [43].

SEM images of cells on HA-B_2O_3-La_2O_3 composite discs after 1 and 7 days of incubation are given in Fig. 7. After 1 day of incubation the cells spread on the surface of the discs, attached to and covered disks sur-

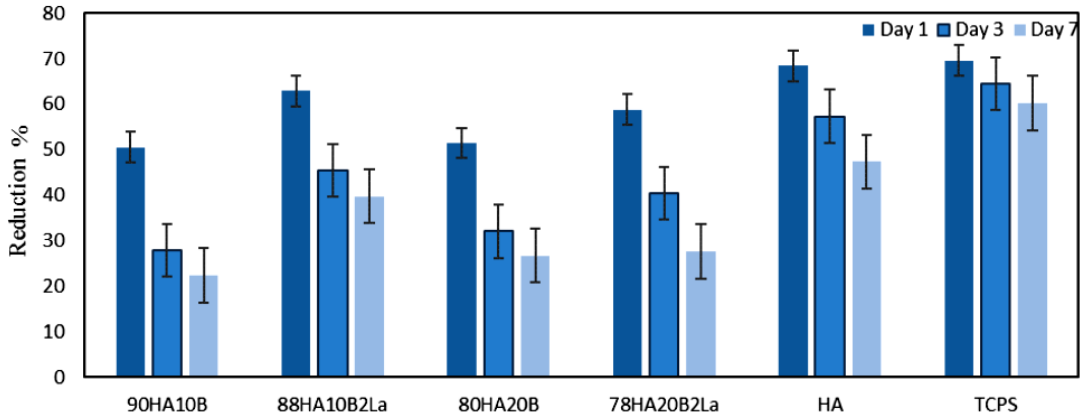

Figure 6. The proliferation rate of cells on pure HA and HA-B_2O_3-La_2O_3 discs (error bars represent standard deviation)

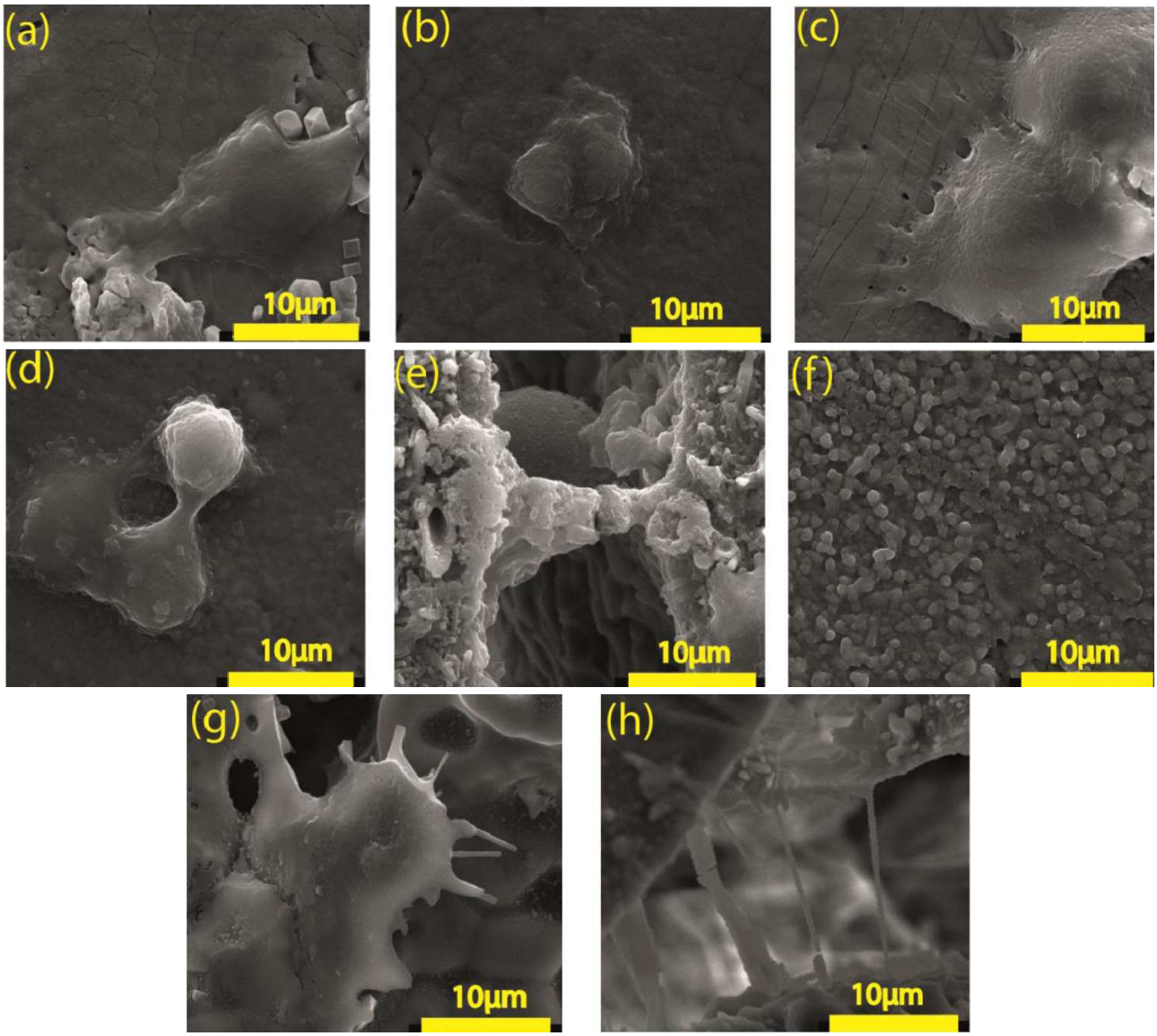

Figure 7. SEM images of Saos-2 cells adhered to surface composites, (a and b) for 90HA10B after incubation time 1 and 7 days respectively, (c and d) for 88HA10B2La after incubation time 1 and 7 days respectively, (e and f) for 80HA20B after incubation time 1 and 7 days respectively, and (g and h) for 78HA20B2La after incubation time 1 and 7 days respectively

face forming layers of cell sheets. Complete coverage indicated that surface properties were ideal for cell attachment and spreading. It was reported that pores and tiny cracks make specific surface area larger and easier to bond with surrounding tissue *in vivo*, thus providing brackets and passages for the growth of the new bone tissue, hence the better biocompatibility [56]. In some SEM images, cell filopodias were broken which was reported to be the result of drying out during the fixation process or a sign of a necrotic cell [57].

IV. Conclusions

Graded HA-B_2O_3-La_2O_3 composites were prepared by wet co-precipitation method with the incorporation of different ratios of B_2O_3 and La_2O_3 as additives. Incorporation of B_2O_3 and La_2O_3 in HA lattice caused an augmentation of the degree of crystallinity and shifting of lattice parameter. The increased sharpness of adsorption peaks in FTIR described the highly crystalline structure as confirmed by the XRD results. SEM images confirmed that incorporation of B_2O_3 and La_2O_3 resulted in an increase in the porosity as well as an increase in the grain size up to 615 nm. Density was decreased with incorporation of B_2O_3 and La_2O_3. 88HA10B2La and 80HA20B composites had the highest tensile strength among all other composites. Furthermore, the incorporation of B_2O_3 and La_2O_3 improved the machinability of HA composites, thus being workable and easy to design. The results from *in vitro* cytotoxicity tests provided clear evidence that 88HA10B2La composites were cytocompatible. Mechanical and biological evaluations of B and La incorporated HA composites (88HA10B2La) indicate that they can be a promising bioceramics implant for use in bone tissue engineering.

References

1. N. Mihailescu, G.E. Stan, L. Duta, M.C. Chifiriuc, C. Bleotu, M. Sopronyi, C. Luculescu, F.N. Oktar, I.N. Mihailescu, "Structural, compositional, mechanical characterization and biological assessment of bovine-derived hydroxyapatite coatings reinforced with MgF_2 or MgO for implants functionalization", *Mater. Sci. Eng. C*, **59** (2016) 863–874.
2. S. Kalmodia, S. Goenka, T. Laha, D. Lahiri, B. Basu, K. Balani, "Microstructure, mechanical properties, and in vitro biocompatibility of spark plasma sintered hydroxyapatite-aluminum oxide-carbon nanotube composite", *Mater. Sci. Eng. C*, **30** [8] (2010) 1162–1169.
3. S.-H. An, T. Matsumoto, H. Miyajima, A. Nakahira, K.-H. Kim, S. Imazato, "Porous zirconia/hydroxyapatite scaffolds for bone reconstruction", *Dental Mater.*, **28** [12] (2012) 1221–1231.
4. T.G.M. Bonadio, F. Sato, A.N. Medina, W.R. Weinand, M.L. Baesso, W.M. Lima, "Bioactivity and structural properties of nanostructured bulk composites containing Nb_2O_5 and natural hydroxyapatite", *J. Appl. Phys.*, **113** [22] (2013) 223505.
5. O. Gunduz, E. Erkan, S. Daglilar, S. Salman, S. Agathopoulos, F. Oktar, "Composites of bovine hydroxyapatite (BHA) and ZnO", *J. Mater. Sci.*, **43** [8] (2008) 2536–2540.
6. S. Ramesh, C.Y. Tan, W.H. Yeo, R. Tolouei, M. Amiriyan, I. Sopyan, W.D. Teng, "Effects of bismuth oxide on the sinterability of hydroxyapatite", *Ceram. Int.*, **37** [2] (2011) 599–606.
7. F. Oktar, S. Agathopoulos, L.S. Ozyegin, O. Gunduz, N. Demirkol, Y. Bozkurt, S. Salman, "Mechanical properties of bovine hydroxyapatite (BHA) composites doped with SiO_2, MgO, Al_2O_3, and ZrO_2", *J. Mater. Sci: Mater Med.*, **18** [11] (2007) 2137–2143.
8. Y.-M. Kong, S. Kim, H.-E. Kim, I.-S. Lee, "Reinforcement of hydroxyapatite bioceramic by addition of ZrO_2 coated with Al_2O_3", *J. Am. Ceram. Soc.*, **82** [11] (1999) 2963–2968.
9. R. Ramachandra Rao, T.S. Kannan, "Synthesis and sintering of hydroxyapatite-zirconia composites", *Mater. Sci. Eng. C*, **20** [1-2] (2002) 187–193.
10. V.V. Silva, F.S. Lameiras, R.Z. Domingues, "Microstructural and mechanical study of zirconia-hydroxyapatite (ZH) composite ceramics for biomedical applications", *Compos. Sci. Technol.*, **61** [2] (2001) 301–310.
11. A. Harabi, E. Harabi, S. Chehlatt, S. Zouai, N.-E. Karboua, L. Foughali, "Effect of B_2O_3 on mechanical properties of porous natural hydroxyapatite derived from cortical bovine bones sintered at 1,050 °C", *Desalination Water Treat.*, **57** (2015) 5303–5309.
12. M. Dzondo-Gadet, R. Mayap-Nzietchueng, K. Hess, P. Nabet, F. Belleville, B. Dousset, "Action of boron at the molecular level: Effects on transcription and translation in an acellular system", *Biol. Trace Elem. Res.*, **85** [1] (2002) 23–33.
13. S.S. Hakki, B.S. Bozkurt, E.E. Hakki, "Boron regulates mineralized tissue-associated proteins in osteoblasts (MC3T3-E1)", *J. Trace Elem. Med. Biol.*, **24** [4] (2010) 243–250.
14. J.H. Lee, C.K. Lee, B.S. Chang, H.S. Ryu, J.H. Seo, K.S. Hong, H. Kim, "In vivo study of novel biodegradable and osteoconductive $CaO\text{-}SiO_2\text{-}B_2O_3$ glass-ceramics", *J. Biomed. Mater. Res. Part A*, **77** [2] (2006) 362–369.
15. X. Yang, L. Zhang, X. Chen, X. Sun, G. Yang, X. Guo, H. Yang, C. Gao, Z. Gou, "Incorporation of B_2O_3 in $CaO\text{-}SiO_2\text{-}P_2O_5$ bioactive glass system for improving strength of low-temperature co-fired porous glass ceramics", *J. Non-Crystal. Solids*, **358** [9] (2012) 1171–1179.
16. Y. Bozkurt, S. Pazarlioglu, H. Gokce, I. Gurler, S. Salman, "Hydroxyapatite lanthanum oxide composites", *Acta Physica Polonica A*, **127** [4] (2015) 1407–1409.
17. R. Fresa, A. Costantini, A. Buri, F. Branda, "Effect of the substitution of La_2O_3 for CaO on the bioactivity of $2.5\,CaO \cdot 2\,SiO_2$ glass", *J. Biomed. Mater. Res.*, **32** [2] (1996) 187–192.
18. W. Lou, Y. Dong, H. Zhang, Y. Jin, X. Hu, J. Ma, J. Liu, G. Wu, "Preparation and characterization of lanthanum-incorporated hydroxyapatite coatings on titanium substrates", *Int. J. Mol. Sci.*, **16** [9] (2015) 21070–21086.
19. A. Tanaka, Y. Nishimura, T. Sakaki, A. Fujita, T. Shin-ike, "Histologic evaluation of tissue response to sintered lanthanum-containing hydroxyapatites subcutaneously implanted in rats", *J. Osaka Dent. Univ.*, **23** [2] (1989) 111–120.
20. F. Fernandez-Gavarron, T. Huque, J.L. Rabinowitz, J.G. Brand, "Incorporation of 140-lanthanum into bones, teeth and hydroxyapatite", *Bone Miner.*, **3** [4] (1988) 283–291.
21. A.Z. Alshemary, A.E. Pazarceviren, A. Tezcaner, Z. Evis, "Mesoporous strontium doped nano sized sulphate hydroxyapatite as novel biomaterial for bone tissue applications", *RSC Adv.*, **6** [72] (2016) 68058–68071.
22. T.J.B. Holland, S.A.T. Redfern, "Unit cell refinement from powder diffraction data: The use of regression diagnostics", *Mineral. Mag.*, **61** [1] (1997) 65–77.
23. A.Z. Alshemary, Y.F. Goh, M. Akram, M.R.A. Kadir, R. Hussain, "Barium and fluorine doped synthetic hydroxyapatite: Characterization and in-vitro bioactivity analysis", *Sci. Adv. Mater.*, **7** [2] (2015) 249–257.
24. A. Tahmasebifar, Z. Evis, "Structural and mechanical characteristics of hydroxyapatite and tri-calcium phosphates doped with Al^{3+} and F^- ions", *J. Ceram. Process. Res.*, **14** [4] (2013) 549–556.
25. J.E. Hilliard, "Estimating grain size by the intercept method", *Metal Progress*, **85** [5] (1964) 99–102.
26. Z. Evis, F. Ozturk, "Investigation of tensile strength of hydroxyapatite with various porosities by diametral strength test", *Mater. Sci. Technol.*, **24** [4] (2008) 474–478.
27. H. Kato, K. Asakura, A. Kudo, "Highly efficient water splitting into H_2 and O_2 over lanthanum-doped $NaTaO_3$ photocatalysts with high crystallinity and surface nanostructure", *J. Am. Chem. Soc.*, **125** [10] (2003) 3082–3089.
28. H. Huppertz, "β-CaB_4O_7: A new polymorph synthesized under high-pressure/high-temperature conditions", *Zeitschrift für Naturforschung B*, **58** [4] (2003) 257–265.
29. Y. Álvarez Criado, M. Alonso, J.C. Abanades, "Composite material for thermochemical energy storage using $CaO/Ca(OH)_2$", *Ind. Eng. Chem. Res.*, **54** [38] (2015) 9314–9327.
30. N. Datta, S. Chatterji, J. Jeffery, A. Mackay, "On the oriented transformation of $Ca(OH)_2$ to CaO", *Mineral. Mag.*, **37** (1969) 250–252.
31. C. Henmi, "Takedaite, a new mineral from Fuka, Okayama Prefecture", *Jpn. Mineral. Mag.*, **59** (1995) 549–552.
32. R.I. Scorei, C. Ciofrangeanu, R. Ion, A. Cimpean, B. Galateanu, V. Mitran, D. Iordachescu, "In vitro effects of calcium fructoborate upon production of inflammatory mediators by LPS-stimulated RAW 264.7 macrophages",

Biol. Trace Elem. Res., **135** [1-3] (2010) 334–344.
33. Z. Evis, B. Yilmaz, M. Usta, S. Levent Aktug, "X-ray investigation of sintered cadmium doped hydroxyapatites", *Ceram. Int.*, **39** [3] (2013) 2359–2363.
34. R. Rajesh, A. Hariharasubramanian, Y.D. Ravichandran, "Chicken bone as a bioresource for the bioceramic (hydroxyapatite)", *Phosphorus Sulfur*, **187** [8] (2012) 914–925.
35. R. Ternane, M.T. Cohen-Adad, G. Panczer, C. Goutaudier, N. Kbir-Ariguib, M. Trabelsi-Ayedi, P. Florian, D. Massiot, "Introduction of boron in hydroxyapatite: synthesis and structural characterization", *J. Alloys Compd.*, **333** [1-2] (2002) 62–71.
36. S. Khoshsima, B. Yilmaz, A. Tezcaner, Z. Evis, "Structural, mechanical and biological properties of hydroxyapatite-zirconia-lanthanum oxide composites", *Ceram. Int.*, **42** [14] (2016) 15773–15779.
37. R.F. Brown, M.N. Rahaman, A.B. Dwilewicz, W. Huang, D.E. Day, Y. Li, B.S. Bal, "Effect of borate glass composition on its conversion to hydroxyapatite and on the proliferation of MC3T3-E1 cells", *J. Biomed. Mater. Res. Part A*, **88** [2] (2009) 392–400.
38. L. Bi, M.N. Rahaman, D.E. Day, Z. Brown, C. Samujh, X. Liu, A. Mohammadkhah, V. Dusevich, J.D. Eick, L.F. Bonewald, "Effect of bioactive borate glass microstructure on bone regeneration, angiogenesis, and hydroxyapatite conversion in a rat calvarial defect model", *Acta Biomater.*, **9** [8] (2013) 8015–8026.
39. S. Jadalannagari, K. Deshmukh, A.K. Verma, R.V. Kowshik, M. Ramanan, S. Roy, "Lanthanum-doped hydroxyapatite nanoparticles as biocompatible fluorescent probes for cellular internalization and biolabeling", *Sci. Adv. Mater.*, **6** [2] (2014) 312–319.
40. M.I. Ahymah Joshy, K. Elayaraja, R.V. Suganthi, S. Chandra Veerla, S.N. Kalkura, "In vitro sustained release of amoxicillin from lanthanum hydroxyapatite nano rods", *Curr. Appl. Phys.*, **11** [4] (2011) 1100–1106.
41. S. Pramanik, B. Pingguan-Murphy, J. Cho, N.A.A. Osman, "Design and development of potential tissue engineering scaffolds from structurally different longitudinal parts of a bovine-femur", *Sci. Reports*, **4** (2014) 5843.
42. R. Ghosh, S. Pal, R. Sarkar, "Study on the development of machinable hydroxyapatite - yttrium phosphate composite for biomedical applications", *Trans. Indian Ceram. Soc.*, **73** [2] (2014) 121–125.
43. S.R. Caliari, D.W. Weisgerber, M.A. Ramirez, D.O. Kelkhoff, B.A. Harley, "The influence of collagen-glycosaminoglycan scaffold relative density and microstructural anisotropy on tenocyte bioactivity and transcriptomic stability", *J. Mech. Behavior Biomed. Mater.*, **11** (2012) 27–40.
44. B.A.C. Harley, H.-D. Kim, M.H. Zaman, I.V. Yannas, D.A. Lauffenburger, L.J. Gibson, "Microarchitecture of three-dimensional scaffolds influences cell migration behavior via junction interactions", *Biophys. J.*, **95** [8] (2008) 4013–4024.
45. H.-W. Kim, Y.-J. Noh, Y.-H. Koh, H.-E. Kim, "Enhanced performance of fluorine substituted hydroxyapatite composites for hard tissue engineering", *J. Mater. Sci.: Mater. Med.*, **14** [10] (2003) 899–904.
46. V. Sarath Chandra, G. Baskar, R. Suganthi, K. Elayaraja, M. Ahymah Joshy, W. Sofi Beaula, R. Mythili, G. Venkatraman, S. Narayana Kalkura, "Blood compatibility of iron-doped nanosize hydroxyapatite and its drug release", *ACS Appl. Mater. Interfaces*, **4** [3] (2012) 1200–1210.
47. B. An, "Dynamic-mechanical thermal analysis - crystallinity and tensile-strength of PBT/ABS blends: their interdependency and variations with ABS content", *Indian J. Chem. Technol.*, **1** [1] (1994) 31–34.
48. B. Demirel, A. Yaras, H. Elcicek, "Crystallization behavior of PET materials", *BAÜ Fen Bil. Enst*, **13** [1] (2011) 26–35.
49. L.L. Hench, J. Wilson, *An Introduction to Bioceramics*, World Scientific, 1993.
50. C. Ergun, "Synthesis and characterization of machinable calcium phosphate/lanthanum phosphate composites", *J. Mater. Process. Technol.*, **199** [1-3] (2008) 178–184.
51. C. Ergun, H. Liu, T.J. Webster, "Osteoblast adhesion on novel machinable calcium phosphate/lanthanum phosphate composites for orthopedic applications", *J. Biomed. Mater. Res. Part A*, **89** [3] (2009) 727–733.
52. A.Z. Alshemary, A.E. Pazarceviren, A. Tezcaner, Z. Evis, "Mesoporous strontium doped nano sized sulphate hydroxyapatite as a novel biomaterial for bone tissue applications", *RSC Adv.*, **6** [72] (2016) 68058–68071.
53. N. Iqbal, M.R. Abdul Kadir, N.H.B. Mahmood, M.F.M. Yusoff, J.A. Siddique, N. Salim, G.R.A. Froemming, M.N. Sarian, H.R. Balaji Raghavendran, T. Kamarul, "Microwave synthesis, characterization, bioactivity and in vitro biocompatibility of zeolite-hydroxyapatite (Zeo-HA) composite for bone tissue engineering applications", *Ceram. Int.*, **40** [10B] (2014) 16091–16097.
54. G. Kaur, G. Pickrell, G. Kimsawatde, D. Homa, H. Allbee, N. Sriranganathan, "Synthesis, cytotoxicity, and hydroxyapatite formation in 27-Tris-SBF for sol-gel based CaO-P_2O_5-SiO_2-B_2O_3-ZnO bioactive glasses", *Sci. Reports*, **4** (2014) 4392.
55. D. Liu, J. Zhang, G. Wang, X. Liu, S. Wang, M. Yang, "The dual-effects of $LaCl_3$ on the proliferation, osteogenic differentiation, and mineralization of MC3T3-E1 cells", *Biol. Trace Elem. Res.*, **150** [1-3] (2012) 433–440.
56. R. Quan, D. Yang, X. Wu, H. Wang, X. Miao, W. Li, "In vitro and in vivo biocompatibility of graded hydroxyapatite-zirconia composite bioceramic", *J. Mater. Sci.: Mater. Med.*, **19** [1] (2008) 183–187.
57. M.A.F. Afzal, P. Kesarwani, K.M. Reddy, S. Kalmodia, B. Basu, K. Balani, "Functionally graded hydroxyapatite-alumina-zirconia biocomposite: Synergy of toughness and biocompatibility", *Mater. Sci. Eng. C*, **32** [5] (2012) 1164–1173.